Neutron and proton transition densities from $^{32,34}S(p,p')$ at $E_p = 318$ MeV. II. Neutron densities for ^{34}S

M. A. Khandaker, J. J. Kelly, P. Boberg, A. E. Feldman, B. S. Flanders,* S. Hyman,† and H. Seifert‡
Department of Physics, University of Maryland, College Park, Maryland 20742

P. Karen, B. E. Norum, and P. Welch
Department of Physics, University of Virginia, Charlottesville, Virginia 22901

S. Nanda and A. Saha
Continuous Electron Beam Accelerator Facility, Newport News, Virginia 23606
(Received 22 July 1991)

Differential cross sections and analyzing powers for low-lying states of ^{34}S were measured using 318 MeV protons. Neutron transition densities for the 2_1^+ and 2_2^+ states were fitted to the data using general expansions which permit evaluation of uncertainties due to statistical and normalization errors, penetrability and distortion, and incompleteness in momentum space. We find that the experimental densities agree well with the shell model for the first 2^+ state, but that the neutron density for the second 2^+ state is distinctly different in shape. We also find $M_n/M_p = +0.27(6)$ for the 2_2^+ state, in qualitative agreement with electromagnetic results for $A = 34$ but in marked disagreement with the shell-model prediction of $M_n/M_p = -0.61$. A detailed analysis of earlier data for 650 MeV, originally described as qualitatively consistent with the shell model, is also presented and shows that these data are more consistent with the present results. The shape of the isoscalar density for the 2_2^+ state of ^{34}S cannot be reproduced with the *sd* shell, supplemented by surface-peaked core polarization, but can be reproduced if an empirical $(1f)^2$ contribution is admitted. Shell-model calculations were performed for other 2^+ and 4^+ states of ^{34}S, but give cross section well below the (p,p') data for all but the lowest 2^+ state. The data for the lowest 1^-, 3^-, and 5^- states in both ^{34}S and ^{32}S are very similar.

I. INTRODUCTION

The *sd* shell has been the subject of intensive investigation within the shell model. The universal *sd* (USD) interaction developed by Brown and Wildenthal is the culmination of a long program seeking an optimal semiempirical shell-model interaction for the *sd* shell fitted to an extensive set of energy-level data [1,2]. The parameters were guided by the *G*-matrix theory of Kuo and Brown [3], which provides initial estimates for fitted matrix elements and constraints upon those parameters which are poorly determined by the available data. It was found necessary to include an $A^{-0.3}$ mass dependence in the matrix elements if the entire shell is to be fitted by a universal interaction; for mass-independent interactions it was previously necessary to subdivide the shell [2]. The resulting interaction reproduces the energy-level data with a standard deviation of about 185 keV.

An important test of the model is its ability to reproduce electromagnetic moments and form factors. Truncation of the shell model to the $(1d_{5/2}, 2s_{1/2}, 1d_{3/2})$ basis must of course be accompanied by renormalization of the transition operators. Brown, Radhi, and Wildenthal fitted effective charges to longitudinal form factors measured with electron scattering for $C2$ and $C4$ transitions in selected nuclei throughout the shell [1]. Thus calibrated, the model was shown to provide a good systematic description of most known $C2$ and $C4$ form factors.

Neutron transition densities measured with proton scattering provide information complementary to the proton densities measured with electron scattering and can provide important new tests of the shell model. Until recently, data for neutron contributions to normal-parity transitions have been largely limited to matrix elements deduced from lifetime measurements assuming isospin symmetry [4] or from analyses of hadron scattering based upon collective or scaling models [5]. While valuable, these techniques yield only a single moment dominated by small densities at large radii. More recently, it has been shown that proton scattering is capable of determining the neutron density with good radial sensitivity provided that the effective interaction is known [6–10]. In the preceding paper, we reported that transition densities fitted to $^{32}S(p,p')$ data at 318 MeV using a suitably calibrated empirical effective interaction agree very well with electroexcitation data, thereby demonstrating the quantitative accuracy of this probe of neutron transition densities [10].

We recently used a similar empirical effective interaction for 180 MeV protons to obtain transition densities for four states of ^{30}Si [9]. For the first two 2^+ states and for the second 4^+ state we found that the neutron transition densities are stronger than shell-model predictions, especially for the second 2^+ and 4^+ states, but for all three positive-parity transitions the shapes of proton and neutron transition densities are similar to each other. For the lowest 3^- state, on the other hand, we found that there is a distinct shape difference between neutron and proton form factors that can be attributed to the contribution of a $2s_{1/2} \rightarrow 1f_{7/2}$ neutron transition.

The second 2^+ state of ^{34}S provides a particularly interesting test of shell-model wave functions because it is one of the few low-lying positive-parity states for which the shell model predicts different signs for the neutron and proton matrix elements [1]. Earlier versions [11] of the interaction also predicted $M_n/M_p < 0$ for the 2_2^+ state of ^{30}Si, but subsequent refinements of the model and use of the USD interaction changed this prediction to $M_n/M_p = 0.26$ for ^{30}Si while still predicting a negative value $M_n/M_p = -0.61$ for the 2_2^+ state of ^{34}S. Due to delicate cancellations, the valence neutron contribution to M_n for the ^{30}Si 2_2^+ state is unusually small, so that the calculated moment is dominated by core polarization contributions. However, the 2_2^+ neutron density determined from ^{30}Si(p,p') at $E_p = 180$ MeV is actually much larger than the shell-model density, suggesting either that the valence wave function is inaccurate or that the simple scaling model of core polarization is inadequate. For ^{34}S, on the other hand, the valence neutron moment is large and negative, $M_n^v = -1.46$, whereas the core contribution is small and positive, $M_n^c = 0.17$. Therefore, ^{34}S provides a unique test of the shell model that should be less vulnerable to inaccuracies due to unusually delicate cancellation between valence and core contributions.

Low-lying 2^+ states in ^{34}S have been studied previously using several reactions. Bernstein *et al.* [12] concluded that the scattering of 650 MeV protons by ^{34}S is consistent with a relative negative sign between M_n and M_p based upon a scaling analysis that neglects shape differences among the densities. Unusual features of the angular distribution for this transition were attributed, without proof, to multistep contributions that might reasonably be expected to become important for relatively weak transitions. However, several subsequent experiments disputed the relative negative sign. From an analysis of the scattering of 120 MeV α particles by ^{26}Mg, ^{30}Si, and ^{34}S, using both distorted-wave Born approximation (DWBA) and coupled-channels (CC) formalisms, Saha *et al.* [13,14] concluded that the M_n/M_p ratios are positive for the 2_1^+ and 2_2^+ states in all three $T=1$ nuclei. Furthermore, channel coupling had little effect upon the cross section to the 2_2^+ state of ^{34}S. From coupled-channels analyses of ^{34}S(p,p') at $E_p = 29.8$ MeV and ^{34}S(n,n') at $E_n = 21.7$ MeV, Alarcon *et al.* [15] also concluded that $M_n/M_p > 0$ for the 2_2^+ state. Although the value deduced for this ratio depends upon the assumptions made concerning the interaction strengths and coupling schemes, the results are clearly inconsistent with the negative sign predicted by the shell model.

Finally, the assumption of isospin symmetry allows both neutron and proton matrix elements to be deduced from electromagnetic lifetime data for a $T=1$ triplet. The magnitude of M_n/M_p is determined by data for mirror nuclei, but the determination of the sign requires data for all three members of the triplet. Combining adopted lifetime data for ^{34}S and ^{34}Ar from the standard compilation [16] with new measurements for ^{34}Cl, Keinonen *et al.* [17] found $M_n/M_p = +0.55 \pm 0.15$. Although this ratio may be subject to Coulombic corrections, its value is clearly positive.

Unfortunately, none of the analysis described above gives any information concerning the shape of the neutron transition density. We have found, as in the case of the 3_1^- state of ^{30}Si, that such information can provide much insight into the structure of a particular transition. Furthermore, the scaling or collective model analyses used in earlier analyses of hadron scattering may produce significant errors in deduced matrix elements if the assumed shapes prove incorrect. The assumption that neutron and proton densities have the same shape may be adequate for the lowest 2^+ state, but will often be quite poor for second and higher 2^+ states without the collective features of the lowest state.

We have measured cross sections and analyzing powers for elastic and inelastic scattering of 318 MeV protons by ^{32}S and ^{34}S [10]. Transition densities were extracted from these data using an empirical effective interaction fitted to data for the inelastic scattering of 318 MeV protons by ^{16}O and ^{40}Ca [18,19]. Neutron transition densities were fitted to the 2_1^+ and 2_2^+ states of ^{34}S using fixed proton densities measured by electron scattering [20]. We find that the neutron and proton matrix elements agree well with previous experiments, but that the shape of the 2_2^+ neutron density is difficult to describe within the confines of the *sd* shell. Nevertheless, the densities we fit to (p,p') at 318 MeV are found to describe the 650 MeV data of Bernstein *et al.* relatively well. Data for other positive-parity states of ^{34}S are compared with shell-model calculations, whereas data for negative-parity states are compared with data for corresponding states of ^{32}S.

The experiment and the procedures used to extract transition densities from proton scattering data were described in the preceding paper [10] and need no further discussion here. The shell-model calculations are described in Sec. II. The extraction of neutron densities for the 2_1^+ and 2_2^+ states of ^{34}S and the comparison between these densities and the shell model is discussed in Sec. III. In Sec. III C we discuss an analysis of the radial densities which suggests that participation of orbitals beyond the *sd* shell is required to reproduce the shape of the isoscalar density for the second 2^+ state of ^{34}S. The 650 MeV (p,p') data are analyzed in Sec. IV. Moments deduced from analyses of other experiments are compared with the present results in Sec. V. The data for negative-parity states of ^{34}S are compared with corresponding data for ^{32}S in Sec. VI. Finally, our conclusions are summarized in Sec. VII.

II. SHELL-MODEL CALCULATIONS

A. Shell-model densities

Shell-model densities may be divided into valence (v) and core (c) contributions [1]

$$\rho_\tau(r) = \rho_\tau^v(r) + \rho_\tau^c(r) , \tag{1}$$

where

$$\rho_\tau^v(r)=\sum_{\alpha,\beta} S_\tau(\alpha,\beta)R_\alpha(r)R_\beta(r)\langle\alpha||Y_J||\beta\rangle\ , \tag{2}$$

$S_\tau(\alpha,\beta)$ is a spectroscopic amplitude, R is a normalized radial wave function, Y_J is a spherical harmonic, and α and β represent the quantum numbers for the particle and the hole, respectively. We used the OXBASH shell-model code [21] and the USD interaction to construct wave functions for 2^+ and 4^+ states of ^{32}S and ^{34}S and to deduce the spectroscopic amplitudes. Good agreement between theoretical and experimental energy levels is obtained for the lowest few 2^+ and 4^+ states of both nuclei, except for the 4_2^+ state of ^{34}S which we did not observe. Harmonic oscillator orbitals with $b=1.881$ fm were used to construct the valence densities, $\rho^v(r)$, and to compute the M_n and M_p moments. The energy levels and moments computed for 2^+ and 4^+ states of ^{34}S are tabulated in Table I.

In principle, the core polarization contribution should be obtained from effective operators, constructed for the particular valence space employed by the shell-model calculation, which incorporate effects due to the excluded portion of the model space [22,23]. In practice, it is more common to fit empirical effective charges to selected data and to assume that the core polarization density either follows the shape of the valence density for each state or is described by a common surface-peaked shape based upon the hydrodynamic model. Given the semiempirical nature of the USD interaction [1], Brown, Radhi, and Wildenthal chose to parametrize the core contribution using a Tassie function [24]

$$C_J(r)\propto r^{J-1}\frac{d\rho_g}{dr}\ , \tag{3}$$

where ρ_g is the ground-state density. It is convenient to normalize C_J according to

$$\int dr\, r^{J+2}C_J(r)=1\ . \tag{4}$$

The core contributions $\rho_\tau^c(r)=M_\tau^c C_J(r)$ are then related to the valence densities using the polarization matrix δ defined by

$$M_p^c=\delta^{pp}M_p^v+\delta^{pn}M_n^v\ , \tag{5a}$$

$$M_n^c=\delta^{np}M_p^v+\delta^{nn}M_n^v\ , \tag{5b}$$

where

$$M_\tau^v=\int dr\, r^{J+2}\rho_\tau^v(r) \tag{6}$$

are valence contributions to the multipole moments M_τ. Brown et al. [1] fitted polarization charges to $C2$ and $C4$ data throughout the *sd* shell assuming that $\delta^{pp}=\delta^{nn}=\delta^{pn}=\delta^{np}=\delta_J$ and found $\delta_2=0.35$ and $\delta_4=0.50$.

Unless otherwise noted, the terms shell model (SM) and shell-model density will be used in this paper to refer to calculations based upon the USD interaction supplemented by this phenomenological model of core polarization. Multipole matrix elements, separated into valence and core contributions, are also tabulated in Table I. As discussed in the Introduction, the model predicts isovector dominance in the valence wave function for the 2_2^+ state of ^{34}S, whence the unusual relative negative sign between neutron and proton matrix elements.

B. Comparison with (p,p') data

Shell-model calculations have been performed for all 2^+ and 4^+ states of ^{34}S below 10 MeV. Table I shows that the shell model accounts for the observed energy levels well and also lists theoretical matrix elements decomposed into valence and core contributions. Proton scattering calculations for the first and second 2^+ states of ^{34}S are compared with the 318 MeV data in Fig. 1. Calculations for the third and fourth 2^+ states and the lowest 4^+ state of ^{34}S are compared with the data in Fig. 2. In these figures, dashed lines represent the contribution of matter densities alone, and solid lines represent full calculations which include the various current and spin densities described in Ref. [25].

We find that the shell model provides very good predictions for the lowest 2^+ state, in both strength and shape, but that the calculation for the second 2^+ state is in marked disagreement with the data. In fact, we probably could not have observed this transition if the shell-model prediction for its strength had been accurate. For both the 2_3^+ and 2_4^+ states we find that the predicted angular distributions have about the correct shape, but that the strengths, particularly for the 2_3^+ state, need considerable enhancement to reproduce the data at low q. This situation is similar to that found for ^{30}Si, for which the shell-model density for the 2_2^+ state has the correct shape but insufficient strength [9]. Similarly, the shell-model calculation for the 4_1^+ state also describes the shape of

TABLE I. Shell-model energy levels (in units of MeV) and matrix elements (in units of fm^J) for ^{34}S.

State J_n^π:	2_1^+	2_2^+	2_3^+	2_4^+	4_1^+	4_2^+	4_3^+	4_4^+
Energy(expt.)	2.127	3.303	4.114	4.889	4.688	6.250	6.729	
Energy(theor.)	2.201	3.138	4.302	4.851	4.896	6.819	6.987	7.623
M_p^v	3.21	1.96	0.80	0.96	35.65	12.30	15.18	27.97
M_p^c	2.51	0.17	0.43	0.44	30.95	16.20	7.82	4.91
M_p	5.72	2.13	1.23	1.40	66.60	28.50	23.00	32.89
M_n^v	3.96	−1.46	0.43	0.29	26.26	20.10	0.45	−18.15
M_n^c	2.51	0.17	0.43	0.44	30.95	16.20	7.82	4.91
M_n	6.47	−1.29	0.86	0.73	57.21	36.30	8.26	−13.24

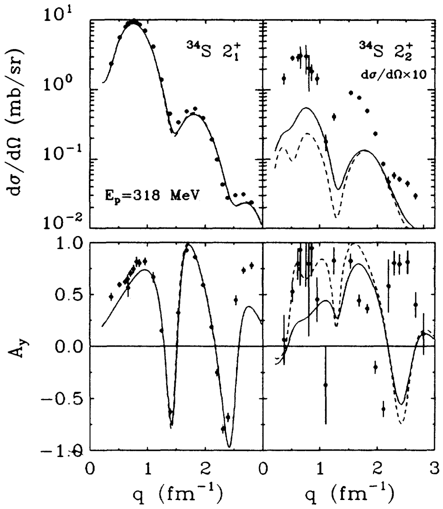

FIG. 1. Calculations for the first and second 2^+ states of ^{34}S using the empirical effective interaction and shell-model wave functions, including core polarization, are compared with data for (p,p') at 318 MeV. Dashed curves include only matter densities and solid curves represent complete calculations.

the angular distribution but the cross section must be multiplied by about 1.5 to match the data.

The effects of nonmatter densities upon calculations for the 2_1^+ state are almost imperceptible at this level and remain small even for third and higher states. Similarly, these contributions are also negligible for the positive-parity states of ^{32}S analyzed in the preceding paper. Only the 2_2^+ state of ^{34}S shows significant sensitivity to current and spin densities due to the destructive interference between ρ_n and ρ_p for this wave function. However, we observe the nonmatter contributions tend to distort the analyzing power calculation for the 2_2^+ state in a manner inconsistent with the data. In fact, the analyzing power data for this state are typical of normal-parity transitions driven by the matter density alone and show no anomalies that might be attributed to other effects.

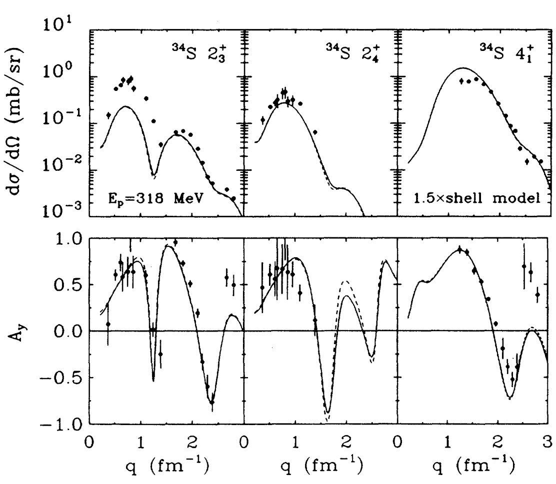

FIG. 2. Calculations for the 2_3^+, 2_4^+, and 4_1^+ states of ^{34}S using the empirical effective interaction and shell-model wave functions, including core polarization, are compared with data for (p,p') at 318 MeV. Dashed curves include only matter densities and solid curves represent complete calculations. The calculation for the 4_1^+ state was scaled by a factor of 1.5.

Current and spin densities for normal-parity states are usually overestimated by shell-model calculations of this kind and are often suppressed by using smaller effective coupling constants. Suppression of current and spin densities is expected for normal-parity excitations as a consequence of the collective nature of core polarization for such transitions. Although no measurements of the transverse form factor for the 2_2^+ state of ^{34}S have been reported, Wördsörfer *et al.* [20] claim that the unusually large transverse form factor predicted by the shell model is incompatible with their (e,e') data. Specifically, they find that form factors for large angles agree with those for smaller angles at matching momentum transfers without need of significant transverse form factors.

Therefore we believe that neglect of current and spin densities is justified for all states of both ^{32}S and ^{34}S for which we have fitted matter or neutron densities. Unfortunately, electron scattering data for ^{34}S are available only for the lowest two 2^+ states. In Sec. III we fit neutron transition densities to the 2_1^+ and 2_2^+ data, but are unable to analyze the data for other positive-parity states without experimental knowledge of their proton transition densities.

III. NEUTRON TRANSITION DENSITIES FOR $^{34}S(p,p')$ AT $E_p = 318$ MeV

A. Fits to the data

Transition charge densities for the 2_1^+ and 2_2^+ states have been fitted to electron scattering data by Wördörfer *et al.* [20]. Proton densities for these states were obtained by unfolding the proton charge form factor. These densities were then used without variation in the analysis of $^{34}S(p,p')$. Fits were made to the proton scattering data using the empirical effective interaction which was reported in Refs. [18] and [19] and which was shown in Ref. [10] to yield results in excellent agreement with known transition densities for ^{32}S. We use the same notation and fitting procedures previously described in detail in Ref. [10].

Elastic scattering calculations for ^{34}S based upon the proton density from Ref. [26] and the assumption $\rho_n \propto \rho_p$ are compared with the data in Fig. 3. The agreement between calculated and experimental cross sections for small momentum transfers confirms the normalization of data taken with the ^{34}S target relative to ^{32}S. The tendency of the cross-section calculation to lie above the data for larger momentum transfers might suggest that the neutron density has a slightly larger radius than proton density for the ground state, but investigation of this pos-

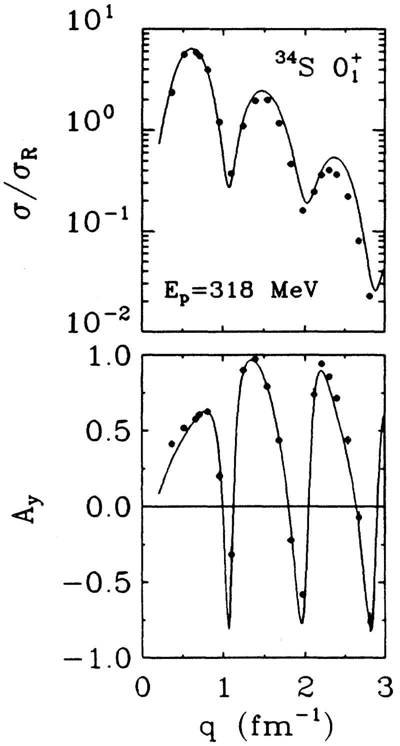

FIG. 3. Elastic scattering data for ^{34}S(p,p') at 318 MeV are compared with calculations based upon the empirical effective interaction, the proton density deduced from electron scattering measurements, and the assumption $\rho_n \propto \rho_p$. The elastic cross section is displayed relative to the Rutherford cross section σ_R to enhance detail.

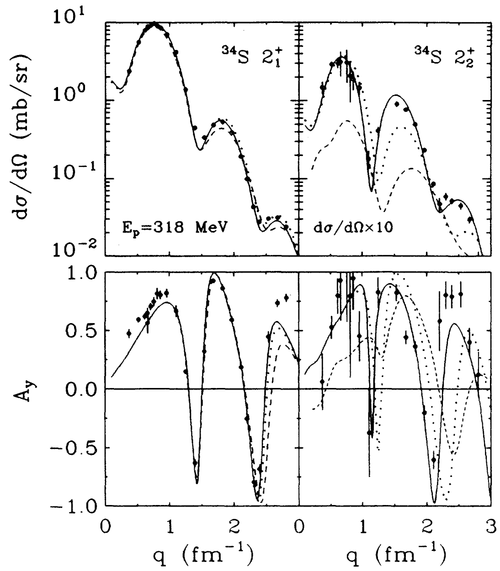

FIG. 4. Fits to the 318 MeV (p,p') data for the 2_1^+, and 2_2^+ states of ^{34}S are compared with shell-model calculations based upon the empirical effective interaction. The dotted lines use (e,e') densities for ρ_p and fit scale factors between ρ_n and ρ_p to the data for $q \leq 1.0$ fm^{-1}, the solid lines represent LGE fits to the (p,p') data for $q \leq 2.7$ fm^{-1}, and the dashed lines show shell-model predictions. Notice that differences between calculations based upon (e,e') or fitted densities are very small for the lowest 2^+ state, but that both scaling and the shell model fail to describe the 2_2^+ angular distribution.

sibility is beyond the scope of this paper.

Two types of fits were made to the inelastic scattering data. First, scale factors between ρ_n and ρ_p were fitted to the data for $q \leq 1.0$ fm^{-1} assuming that these densities are proportional. Second, LGE expansion coefficients for the neutron transition density were fitted to the data for $q \leq 2.7$ fm^{-1} holding the proton density obtained from electron scattering fixed. These fits are compared with the data in Fig. 4 and the densities are compared with the shell model in Fig. 5. The scale factor results are shown as dotted lines and shell-model predictions are shown as dashed lines. Expansion coefficients for neutron densities fitted to ^{34}S(p,p') are collected in Table II.

We find that both the scale factor analysis and the shell-model prediction agree very well with the data for the lowest 2^+ state of ^{34}S. For this state, both ρ_p and ρ_n have simple and similar shapes that are easily described by the shell model. The M_n/M_p results for the 2_1^+ state are 1.07(7) for the LGE or 1.07(10) for the scale factor analysis. These results agree both with each other and with the shell-model prediction of 1.13. The data for the second 2^+ state are more interesting. The ratio between second and first cross-section maxima is much larger for the 2_2^+ than for the 2_1^+ state, suggesting a transition density of more interior or more complicated shape. Unlike

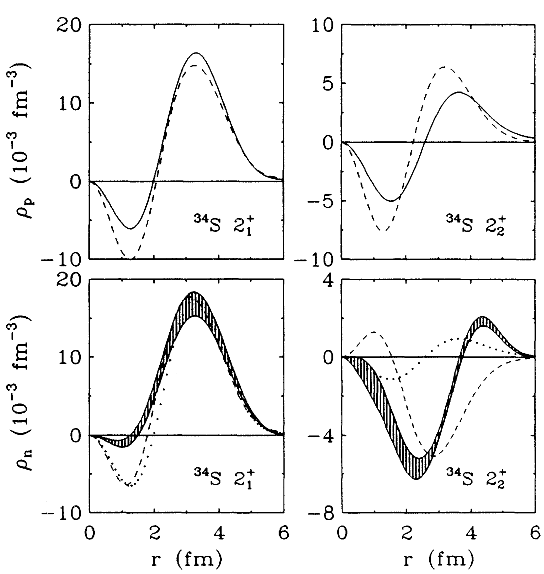

FIG. 5. Proton and neutron transition densities fitted to data for the 2_1^+ and 2_2^+ states of ^{34}S, shown as solid lines or bands, are compared with shell-model predictions, shown as dashed lines. The dotted curves show neutron densities fitted assuming proportionality between ρ_n and ρ_p.

TABLE II. Neutron transition density parameters for ^{34}S. LGE coefficients a_n are in units of fm^{-3} and are based upon $b=1.881$ fm. The units of M_n are fm^J and the units of R_n are fm.

n	2_1^+	2_2^+
0	$(4.860\pm0.49)\times10^{-2}$	$(-1.426\pm0.12)\times10^{-2}$
1	$(-2.818\pm0.24)\times10^{-2}$	$(-1.751\pm0.69)\times10^{-3}$
2	$(5.211\pm0.37)\times10^{-3}$	$(3.396\pm0.32)\times10^{-3}$
3	$(6.584\pm1.35)\times10^{-4}$	$(-3.489\pm1.37)\times10^{-4}$
4	$(-5.560\pm0.63)\times10^{-4}$	$(-4.503\pm0.99)\times10^{-4}$
5	$(0.594\pm2.32)\times10^{-5}$	$(4.168\pm5.64)\times10^{-5}$
6	$(8.790\pm1.70)\times10^{-5}$	$(1.062\pm0.44)\times10^{-4}$
7	$(-1.813\pm0.71)\times10^{-5}$	$(0.702\pm2.63)\times10^{-5}$
8	$(-1.333\pm0.54)\times10^{-5}$	$(-2.373\pm1.97)\times10^{-5}$
9	$(3.795\pm2.96)\times10^{-6}$	$(-1.380\pm1.35)\times10^{-5}$
10	$(3.498\pm2.35)\times10^{-6}$	$(-3.254\pm6.01)\times10^{-6}$
11	$(-1.001\pm8.77)\times10^{-7}$	$(-0.534\pm1.31)\times10^{-6}$
M_n	6.65 ± 0.40	0.61 ± 0.14
R_n	4.20 ± 0.19	5.82 ± 0.84

the 2_1^+ state, the scale factor analysis fails to describe the data for $q>1$ fm^{-1}, indicating a significant shape difference between ρ_n and ρ_p. The neutron density fitted using the more general LGE model describes both cross section and analyzing power data for the 2_2^+ state very well. Nevertheless, when the scale factor analysis is restricted to $q\leq1.0$ fm^{-1}, the ratio of $+0.22(6)$ agrees well with the LGE result of $M_n/M_p=0.27(6)$ but disagrees strongly with the shell-model prediction $M_n/M_p=-0.61$.

We studied the sensitivity of deduced neutron densities to uncertainties in the isovector components of the effective interaction by performing fits based upon several variations of the isovector interaction. These variations included omission of the isovector interaction, use of the Franey-Love (FL) t matrix [27] without density dependence, use of the isovector component of the LR interaction due to Ray [28], or use of the Paris-Hamburg [29] (PH) version of the isovector interaction. The resulting variations of the fitted densities always lie within the quoted error bands. Similar results have been obtained for neutron densities fitted to ^{48}Ca(p,p') at either 200 or 318 MeV, independently or simultaneously [30]. Given that medium modifications to the isovector effective interaction at 318 MeV are expected to be quite small [29] and that the net contribution of this isovector interaction is much smaller than the contribution of the isoscalar interaction even in the presence of a significant isovector density, inaccuracies of theoretical estimates of medium modifications to the isovector interaction have little impact upon the accuracy of fitted densities. Except for $q<0.5$ fm^{-1} and for the immediate vicinity of minima, the relative contribution of the isovector interaction to the cross section for the 2_2^+ state of ^{34}S is no more than a few percent for $0.5<q<3.0$ fm^{-1}. Even in the minima, the 10–20% isovector contributions do not significantly affect the analysis. Isovector contributions for the other states analyzed are even less influential. Therefore the fitted densities are independent of reasonable variations of the isovector interaction.

We also studied the sensitivity of fitted neutron densities to possible ambiguities in the isoscalar interaction by performing fits for each of the models discussed in Ref. [10]. In that paper we demonstrated that use of the empirical effective interaction provides the most accurate extraction of transition densities for ^{32}S which were already known from electroexcitation measurements. Use of theoretical interactions gives similar but less accurate results. In the present analysis for ^{34}S(p,p'), we again find that both theoretical and empirical density-dependent interactions give similar neutron transition densities even for the 2_2^+ state. The bimodal shape and the positive sign of M_n for the 2_2^+ neutron density are independent of reasonable variations of the effective interaction. We limit our presentation of fitted densities to the empirical interaction, which is expected to give the most accurate results.

B. Comparison of densities and form factors with the shell model

The transition density for the 2_2^+ state of ^{34}S is compared with the shell model and the scaled proton density in Fig. 5. Plots of $r^{J+2}\rho(r)$ are displayed in Fig. 6. Although the fitted density appears to be negative over most of its range, the integral moment $M_n=+0.61$ is positive because the moment weights the density with r^{J+2} and emphasizes the positive lobe at large radii. In order to reproduce the low-q cross section, the scale factor analysis also requires positive $M_n=+0.50$ but lacks the strong negative lobe in interior needed to fit the high-q data. Although the shell-model density displays a negative lobe similar in strength to the fitted density, it lacks the node at about 3.7 fm and the positive surface lobe. Thus, the shell model fails to achieve sufficient cross section because $M_n=-1.29$ remains negative and interferes destructively with M_p to yield a very small $M_0=0.84$, as compared with 2.87 in the LGE model.

Form factors for the charge and neutron densities for these states are compared with the shell model in Fig. 7.

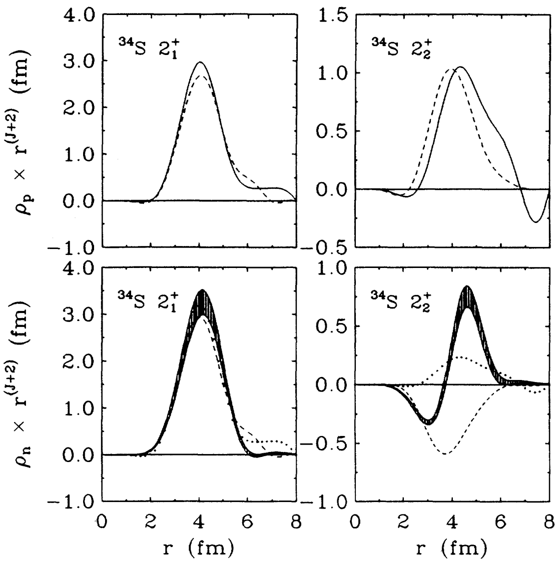

FIG. 6. Proton and neutron transition densities fitted to data for the 2_1^+ and 2_2^+ states of ^{34}S, shown as solid lines or bands, are compared with shell-model predictions, shown as dashed lines. The dotted curves show neutron densities fitted assuming proportionality between ρ_n and ρ_p. The densities were scaled by r^{J+2} to emphasize features relevant to traditional geometric moments of the transition density.

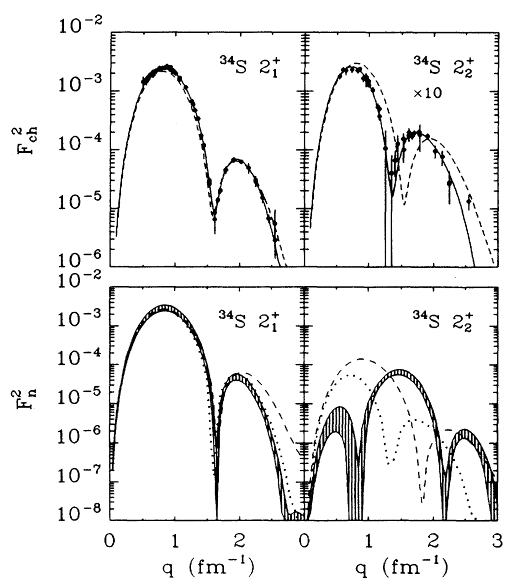

FIG. 7. Charge and neutron form factors fitted to data for the 2_1^+ and 2_2^+ states of ^{34}S, shown as solid lines or bands, are compared with shell-model predictions, shown as dashed curves. Neutron form factors fitted under the assumption $\rho_n \propto \rho_p$ are shown by dotted lines. The charge form factors were corrected for distortion and are plotted against the effective momentum transfer.

The FOUBES code [31] was used to perform distortion corrections to the (e,e') data and to the charge form factors, as described in Ref. [10]. The shell model describes the charge form factor for the lowest 2^+ state quite well, but even though it reproduces the transition strength for the second state it fails to describe the shape of its form factor. Similarly, the shell model describes the shape of the neutron form factor we deduced for the lowest 2^+ state over its first maximum but is larger for $q > 2$ fm^{-1}. More interestingly, the shell model dramatically fails to describe the shape of the neutron form factor for the second state. Each node in the squared form factor represents a sign change in the Fourier transform of the density. The shell model predicts that the relative sign between neutron and proton form factors for small momentum transfer q is negative and that the nodes occur at similar momentum transfers, so that the relative negative sign persists for most q. The experimental form factor, on the other hand, begins positive but develops a node at small momentum transfer, $q \approx 0.8$ fm^{-1}, due to the strong surface lobe in the fitted density. It is worth noting that the node in the experimental charge form factor also occurs at significantly lower q than predicted by the shell model, although this effect is certainly larger for the neutron form factor. The third maximum in the experimental form factor occurs at relatively large momentum transfer and originates in the constructive interference between the two lobes of the transition density.

It is also worth noting that the somewhat peculiar features displayed by the $r^{J+2}\rho_p(r)$ curves shown in Fig. 6 are present in the published parametrization of the transition charge densities also and are *not* introduced by deconvolution of the proton form factor from a density confined by the Fourier-Bessel expansion to $r \le R$, where here $R = 8.0$ fm. Also note that the oscillations that appear in the 2_1^+ shell model density at large radii arise from corresponding oscillations in the ground-state charge density upon which the core polarization shape is based. Close examination of most published transition charge densities reveals similar vagaries which cast doubt upon the reliability of the unrealistically small uncertainties often quoted for matrix elements and transition radii, quantities which emphasize densities at large radii that are not strongly constrained by electron scattering data. These implausible structures are suppressed in our (p,p') analysis by careful application of the tail bias.

C. Discussion

1. Model space

The role configurations outside the *sd* shell might play in explaining the unusual surface lobe observed in the 2_2^+ neutron density can be investigated using a schematic shell-model density of the form

$$\rho_\tau(r) = \sum_{\alpha\beta} \chi_{\alpha\beta}\rho_{\alpha\beta}(r) , \tag{7}$$

where

$$\rho_{\alpha\beta}(r) = (1+\delta_\tau)^{-1}[\rho^v_{\alpha\beta}(r) + \delta_\tau C_J(r)] \tag{8}$$

represents the radial shape of the single-particle transition $\beta\leftrightarrow\alpha$. It is convenient to normalize both valence and core shapes to unit moment

$$\int dr\, r^{J+2}\rho^{v}_{\alpha\beta}(r)=\int dr\, r^{J+2}C_J(r)=1 \tag{9}$$

so that $\chi_{\alpha\beta}$ represents the contribution of the $(\alpha\beta)$ configuration to the net multipole moment. For simplicity, we assume that spin-orbit partners have the same radial wave functions so that $\alpha=(n_\alpha l_\alpha)$ suffices to specify the orbital. The valence densities $\rho^{v}_{\alpha\beta}(r)\propto R_\alpha(r)R_\beta(r)$ were computed using oscillator wave functions. The core density $C_J(r)$ was computed using the Tassie model. It is simplest to apply this model to isospin densities ρ_0 and ρ_1 because the assumption of charge independence for core polarization can be implemented with only a single nonvanishing effective charge δ_0 for each multipolarity J. We use $\delta_0=0.70$ for 2^+ states. Application to nucleon densities ρ_p and ρ_n requires coupling between these densities or independent values of δ_p and δ_n.

Figure 8 compares experimental isospin densities (bands) for low-lying 2^+ states of ^{34}S with the original shell-model predictions (dashed lines) and with unweighted least-squares fits of the schematic model described by Eqs. (7) and (8) to the experimental densities for $r<6$ fm. The dotted curves were obtained within the *sd* shell and thus are described by the two parameters χ_{dd} and χ_{ds}. The solid curves were obtained by expanding the basis to include $(1f)^2$ configurations represented by a third parameter χ_{ff}. The fitted parameters are listed in Table III.

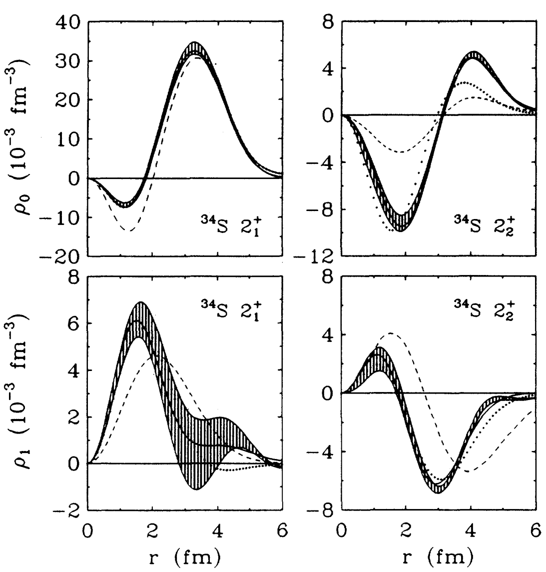

FIG. 8. Experimental densities (bands) for 2^+ states of ^{34}S are compared with the shell-model densities (dashed) and with fits to the experimental densities based upon Eq. (7). Fits limited to the *sd* shell are shown as dotted lines and fits including the f^2 configuration are shown as solid lines. Calculated densities include core polarization estimates based upon the Tassie model. The dotted and solid lines employ an oscillator parameter $b=1.99$ fm that was chosen to optimize the two-parameter fit to ρ_0 for the 2_1^+ state.

Unfortunately, the values of χ_{ff} obtained for the 2_1^+ states of both ^{32}S and ^{34}S depend strongly upon the oscillator parameter b. When these densities are fitted using the value $b=1.881$ fm expected for the sulfur isotopes, good qualitative agreement is obtained using two parameters χ_{dd} and χ_{ds}, but quantitative agreement requires unreasonably large values for χ_{ff}. The problem is that ρ_{ff} and ρ_{dd} are sufficiently similar in shape, with ρ_{ff} peaking at slightly larger radius, that a small outward shift of the density obtained in the two-component model can be accomplished by shifting much of the strength from χ_{dd} to χ_{ff}. Thus it is likely that small modifications to the shapes of the valence orbitals or to the Tassie model of core polarization could explain the remaining differences between the two-component model and the experimental densities. Therefore, to reduce ambiguities in the interpretation of χ_{ff}, we varied b so that the best fit to ρ_0 for 2_1^+ states can be obtained within the two-component model. For ^{34}S this procedure suggests a modest increase of the oscillator parameter to $b=1.99$ fm, perhaps due to deficiencies in oscillator wave functions. Note that although model dependence obviates strict interpretation of the $\chi_{\alpha\beta}$ coefficients, the parametrizations do reproduce the densities relatively well.

We find that the two *sd*-shell amplitudes suffice to describe the important qualitative features of all the 2^+ densities observed except the strength of the isoscalar density observed at large radii for the 2_2^+ state of ^{34}S. In fact, variation of the oscillator parameter to fit ρ_0 for the 2_2^+ state in the two-component model requires an absurdly large value, $b=2.41$ fm. This failure of the two-component model to describe the isoscalar 2_2^+ density of ^{34}S indicates that configurations outside the *sd* shell play a significant role in this transition. It is interesting to observe that the two-component fit lies intermediate between the shell model and the experimental densities, but is unable to reproduce the strengths of both the interior and the surface lobes simultaneously. The enhanced surface lobe can be reproduced using a strong χ_{ff} contribution that interferes destructively with a similarly strong χ_{dd} contribution. However, the $\chi_{\alpha\beta}$ coefficients themselves must be interpreted with caution because reasonable variations of the model assumptions can produce large variations of the fitting parameters when near cancellation of similar shapes is involved. Nevertheless, we consider the evidence for f^2 participation to be strong enough to warrant expansion of the model space.

2. *Effective operators*

Within the *sd* shell, $C4$ densities are characterized by a unique $1d\leftrightarrow 1d$ shape which suffices to describe the shape of experimental densities relatively well. However, the contrast between scale factors relating shell-model predictions for $C4$ excitations to the data for ^{32}S and ^{34}S is significant. Similarly, the shell model describes the strengths of the (e,e') form factors for the 4_1^+ state of ^{28}Si

TABLE III. Comparison between shell-model (SM) amplitudes and fits to experimental densities for low-lying 2^+ states in ^{34}S. The fits are based upon $b=1.991$ fm. Fit I includes configurations only within the *sd* shell and Fit II includes $(1f)^2$ configurations in addition to the *sd*-shell basis.

State	Density		χ_{dd}	χ_{ds}	χ_{ff}
2_1^+	ρ_0	SM	5.55	8.10	
		Fit I	8.72	5.35	
		Fit II	8.73	5.36	0.00
2_1^+	ρ_1	SM	1.52	−0.68	
		Fit I	1.31	−1.29	
		Fit II	0.31	−1.66	2.22
2_2^+	ρ_0	SM	−1.55	2.50	
		Fit I	−2.86	4.14	
		Fit II	−7.05	2.53	7.61
2_2^+	ρ_1	SM	−1.44	−2.39	
		Fit I	−1.44	−0.77	
		Fit II	−2.27	−1.08	1.86

and the 4_2^+ state of ^{30}Si relatively well, but is more than a factor of 2 below the ^{30}Si$(p,p')4_2^+$ cross-section data at $E_p=180$ MeV [9]. For the latter state, the shell model predicts $M_n/M_p=0.42$, but the LGE fit to the data gave 1.08(13). Therefore, the model requires much larger normalization factors for the neutron-excess case than for the self-conjugate case.

These observations suggest that the model predictions for isovector amplitudes are seriously in error, either through valence configurations or through the assumption of charge independence for core polarization, and that significant deficiencies are evident for both $C2$ and $C4$ excitations. It will be of interest to perform similar analyses for nuclei in the lower half of the *sd* shell to determine whether shell-model matrix elements involving the $d_{3/2}$ orbital are specifically suspect. The $C2$ radial densities also clearly indicate that the basis must be expanded to describe even relatively low-lying states of the sulfur isotopes. Finally, the somewhat arbitrary assumptions concerning core polarization densities must be evaluated by comparison with microscopic calculations of effective operators.

IV. ANALYSIS OF ^{34}S(p,p') AT $E_p=650$ MeV

The original claim by Bernstein *et al.* [12] that the scattering of 650 MeV protons by ^{34}S is consistent with the negative M_n/M_p predicted by the shell model for the second 2^+ state was responsible for considerable experimental interest in that state. Hence, it is of interest to use the present densities for calculations at 650 MeV. However, Bernstein *et al.* relied upon ratios between the cross sections for the 2_1^+ and 2_2^+ states and presented only smoothed curves with arbitrary normalization. In this section we analyze their original cross section and analyzing power data and determine the normalization relative to calculations for the 2_1^+ state, for which the nuclear structure is known with little ambiguity.

A. Calibration of the 650 MeV interaction

First it is necessary to calibrate the effective interaction for 650 MeV protons. Miskimen *et al.* [32] show that IA calculations for the 2_1^+ state of ^{28}Si based upon the FL t matrix and a transition density fitted to (e,e') data produce a minimum at a momentum transfer that is too small. Similar discrepancies are also found for inelastic scattering calculations for ^{40}Ca based upon (e,e') densities [33]. Unpublished analyzing power calculations and data [34] show dramatic low-q discrepancies reminiscent of the famous results for ^{40}Ca elastic scattering at 500 MeV [35]. Finally, using either a free interaction or a theoretical density-dependent effective interaction, Ray finds that the calculated angular distribution for elastic scattering from ^{16}O must still be shifted toward significantly higher momentum transfer if it is to reproduce the data [28].

We found that similar defects of nonrelativistic elastic and inelastic scattering calculations for ^{16}O and ^{40}Ca at 500 MeV could be corrected using an empirical effective interaction of the same form fitted to data for lower energies [36]. Furthermore, the optical potentials calculated from the effective interaction fitted to inelastic scattering are very similar to Schrödinger-equivalent potentials deduced from either Dirac phenomenology [37] or the IA2 version [38] of the Dirac impulse approximation. Therefore, we attempted to fit a similar empirical effective interaction to the data for 650 MeV proton scattering. The only inelastic scattering data for self-conjugate targets that is available at this energy is limited to states with surface-peaked transition densities and momentum transfers between 0.8 and 1.8 fm^{-1} and are of relatively low quality. These data alone do not uniquely determine the effective interaction. Therefore, we generalized the fitting procedures to accommodate elastic scattering and include the high-quality elastic data [39] available for ^{16}O together with lower-quality elastic data for ^{28}Si and ^{40}Ca and inelastic data [32–34] for the 2_1^+ state of ^{28}Si and the

2_1^+, 3_1^-, 3_2^-, 3_3^-, and 5_1^- states of ^{40}Ca simultaneously. Details of the model and fitting procedure may be found in Refs. [19] and [36]. Using $\mu_1 = 2.5$ fm^{-1} and $\mu_3 = 6.0$ fm^{-1}, based upon a reparametrization of the LR interaction for this energy, a fit to cross section and analyzing power angular distributions for nine states yields the parameters $b_1 = 162.8$ MeV fm^3, $S_2 = 0.89$, $d_2 = -0.20$, $S_3 = 0.70$, and $b_3 = 6.56$ MeV fm^3. Note that $S_1 = 1.0$ was held constant because these data are relatively insensitive to its value. This set of parameters is very similar to the results obtained previously for 500 MeV [36].

To illustrate the quality of the fit, we compare elastic scattering calculations for ^{16}O based upon the FL, LR, and empirical interactions with the data in Fig. 9. We find that the empirical effective interaction successfully describes the shift of the cross-section angular distribution toward larger q and the suppression of the analyzing power for low q that is characteristic of nonrelativistic calculations for proton elastic scattering above 300 MeV. Note that the analysis was limited to $q \leq 2.7$ fm^{-1} because of limitations in the knowledge of form factors for high q. The success of this analysis suggests that results of comparable accuracy should be possible for other transitions at this energy if the structure is known. Also note that the elastic cross-section calculations using the empirical interaction are quite accurate for small momentum transfers, but that the FL and LR calculations fall significantly below the data.

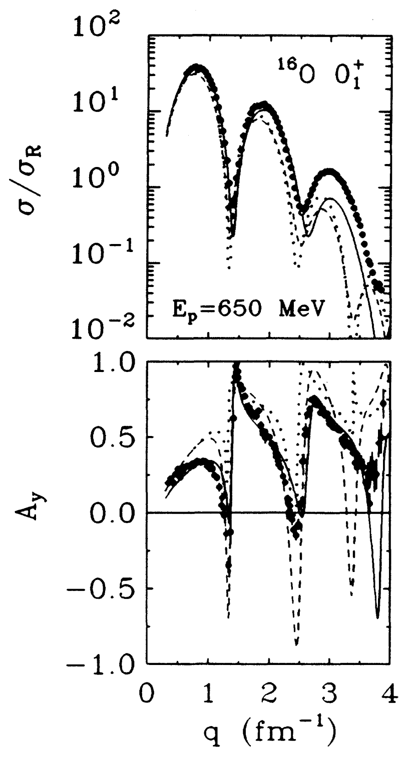

FIG. 9. Data for elastic scattering of 650 MeV protons by ^{16}O are compared with calculations based upon the FL interaction (dotted lines), the LR interaction (dashed lines), and an empirical effective interaction fitted to data for nine states simultaneously. The elastic cross section is displayed relative to the Rutherford cross section σ_R to enhance detail.

B. Normalization of the ^{34}S(p,p') data for 650 MeV

Calculations for ^{34}S(p,p') at 650 MeV based upon shell-model densities and the densities fitted to (p,p') data at 318 MeV are compared with the data in Fig. 10. Because the experimental cross sections for both elastic scattering and for the 2_1^+ state are substantially smaller than expected, we found it necessary to scale all of the 650 MeV ^{34}S cross-section data by a factor of 1.4. The original data are shown as open circles and the renormalized data by filled circles. We find that calculations based upon the (e,e') proton densities and the neutron densities fitted to (p,p') at 318 MeV describe the renormalized 650 MeV data for elastic scattering and the 2_1^+ state very well. Although a renormalization factor of 1.4 may appear to be rather large, we note that the target, consisting of sulfur powder and a 10% lucite binder, may present difficult normalization problems, such as sublimation. We believe that the low-q scattering calculations for both the ground state and the 2_1^+ state should be more accurate than the original normalization of the 650 MeV data, especially considering that the original normalization of these data was not published. Therefore, we feel justified in renormalizing the experimental cross sections accordingly.

The shell-model calculation for the 2_1^+ state is also in good agreement with the renormalized data, as it is for the 318 MeV data also. By contrast, the shell-model calculation for the 2_2^+ state is more than a factor of 4 below the first peak of the cross section and its node occurs at too large a momentum transfer. Very similar deviations are also observed at 318 MeV (Fig. 1). However, although the shape of the 2_2^+ angular distribution at 650 MeV is described relatively well by the calculation based upon the density fitted to the 318 MeV data, there appears to be a residual discrepancy at both peaks. We also note that the dip in the data at the peak of the 2_2^+ angular distribution is probably artificial and may be due to experimental difficulties in extracting a small peak from the much larger ^{12}C elastic scattering peak due to the lucite binder. Despite our reservations concerning the quality of these data, we present fits in the next section which demonstrate conclusively that there is no important qualitative disagreement between the two experiments (provided that the 650 MeV data are properly renormalized).

C. Neutron densities fitted to ^{34}S(p,p') at 650 MeV

Fits of 650 MeV data were made for several values of the renormalization factor between 1.0 and 1.4; the results for the former are shown in Fig. 11 and for the latter in Fig. 12. Using the original normalization, the fitted density for the 2_1^+ state is similar in shape but about a factor of 0.8 smaller than the corresponding results for 318 MeV. Using the more likely normalization factor of 1.4, the fitted density is in good agreement with the 318 MeV result for the 2_1^+ state. For the 2_2^+ state, on

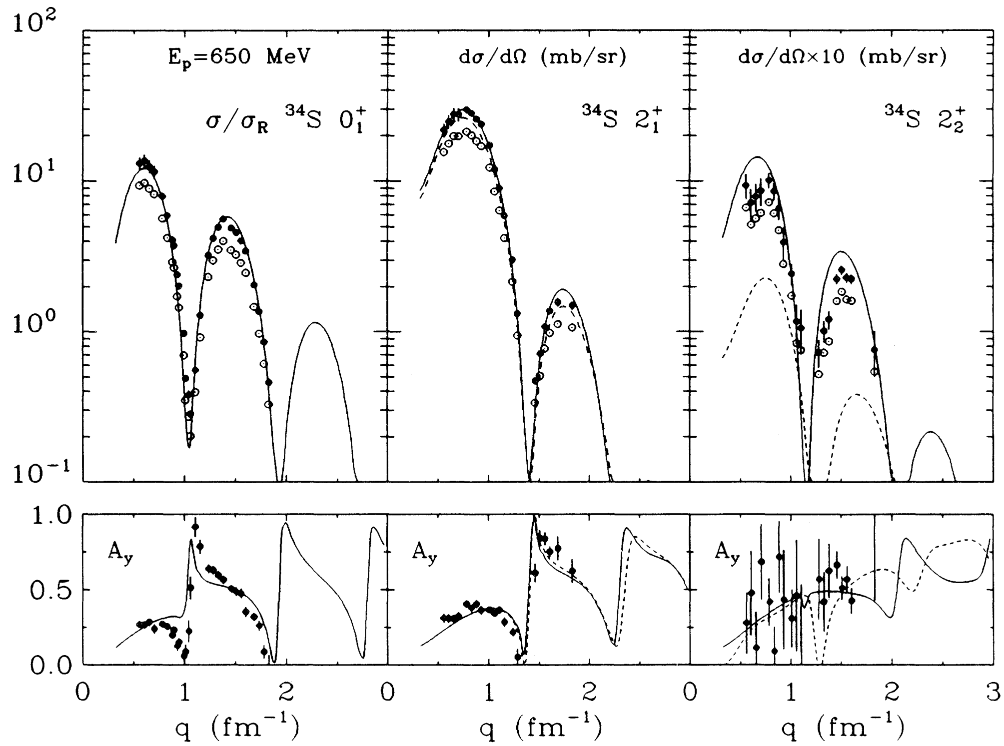

FIG. 10. Calculations for ^{34}S(p,p') at 650 MeV based upon the empirical effective interaction are shown as solid lines and are compared with the data of Bernstein *et al.* (Ref. [12]). The original data are shown as open circles and data that have been renormalized by the factor of 1.4 required to match the peak of the 2_1^+ calculation are shown as filled circles. Calculations using shell-model densities are shown by dashed lines.

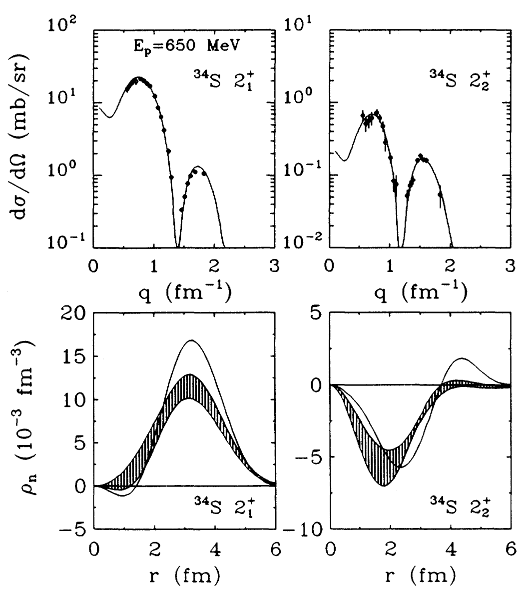

FIG. 11. Cross sections and densities fitted to the 650 MeV data using the original normalization. For densities the solid lines show the fits to the 318 MeV data. Without renormalization the 650 MeV fit gives a smaller density for the 2_1^+ state.

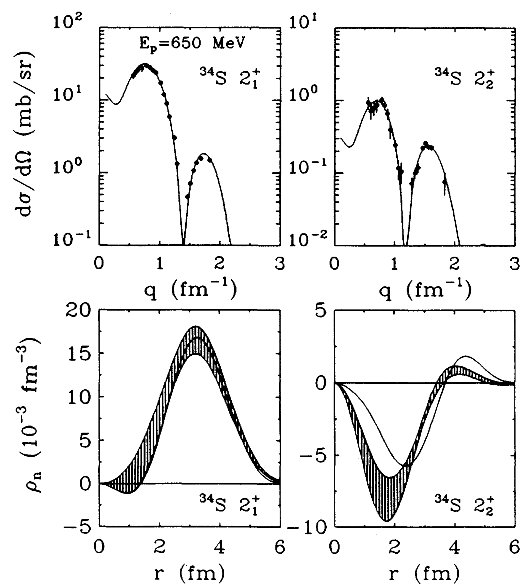

FIG. 12. Cross sections and densities fitted to the 650 MeV data renormalized by a factor of 1.4. For densities the solid lines show the fits to the 318 MeV data. With renormalization the 650 MeV fit gives good agreement with the 318 MeV result for the 2_1^+ state, but the 2_2^+ density remains compressed to smaller radii.

the other hand, the fit to the original 650 MeV data is similar to the 318 MeV result in the interior but lacks the surface lobe. Finally, the fit to the scaled data does produce a surface lobe, but that feature is somewhat less prominent and occurs at a slightly smaller radius than the corresponding density fitted to the 318 MeV data. However, it is worth noting that the suspect data points at the peak of the 2_2^+ angular distribution tend to reduce the low-q strength of the fitted form factor and to reduce the surface lobe of the density.

It is instructive to examine the form factor for the fitted neutron densities. The 650 and 318 MeV form factors are compared in Fig. 13 with the shell-model prediction for the 2_2^+ state. The error band on the 650 MeV form factor is relatively narrow in the region where there are data, but widens dramatically for momentum transfers both below and above the range of the data. Fairly good agreement between the two fits is obtained for intermediate momentum transfers, but the 650 MeV fit lacks both the low-q and high-q features of the 318 MeV fit for which more complete data were available. A band this wide does not seriously exclude additional form factor peaks.

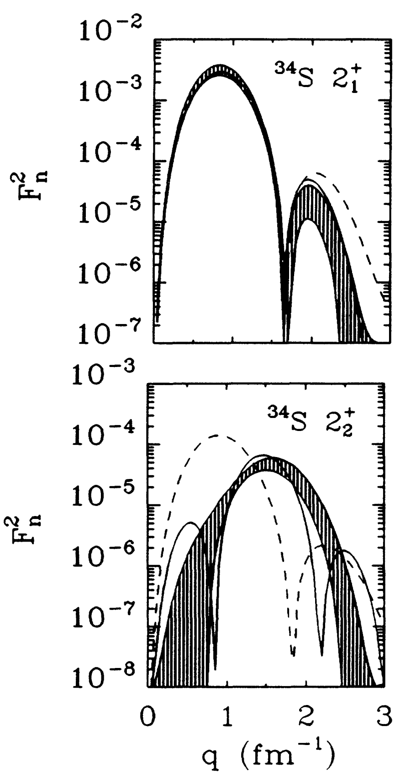

FIG. 13. Form factors representing the neutron densities for the 2_1^+ and 2_2^+ states of ^{34}S: the bands correspond to fits to the renormalized data for 650 MeV, the solid lines to the 318 MeV results, and the dashed lines to the shell-model predictions. Good agreement between the two analyses is obtained for the 2_1^+ state. Relatively good agreement is obtained for the 2_2^+ in the range of momentum transfer for which there are 650 MeV data, but the error band widens rapidly beyond that range.

We have also performed combined fits to the data for 318 MeV and the scaled 650 MeV data simultaneously. The results for the 2_1^+ state are indistinguishable from the fit to the 318 MeV data alone, confirming the renormalization of the 650 MeV data. The results for the 2_2^+ state are more complicated. For low momentum transfer the 650 MeV data pull down the form factor so that the combined fit falls below the 318 MeV data at and below the first peak, a region where the single-energy fit to that data was more successful. On the other hand, the combined fit reproduces the 318 MeV datum at the second peak more accurately than did the single-energy fit. These fits are illustrated in Fig. 14, where the solid lines represent the dual-energy fit to both data sets simultaneously, the long-dashed line calculations based upon the fit to the 650 MeV data alone, and the short-dashed line calculations based upon the fit to the 318 MeV data alone. We find that the dual-energy fit provides a good description of both data sets, although both single-energy fits do produce slightly better χ^2 for the appropriate data set. Therefore, we conclude that there does exist a neutron transition density compatible with both sets of data. However, inasmuch as we have had to renormalize the 650 MeV data and judge that set inferior to the 318 MeV data, we claim that the single-energy fit to the 318 MeV data is more reliable and decline to present the LGE coefficients for fits that include the 650 MeV data.

The single- and dual-energy 2_2^+ densities are compared in Fig. 15, where to reduce clutter only the combined fit carries an error band. The only significant difference between the dual-energy result and the 318 MeV density is found at large radii where the deficit at the peak of the

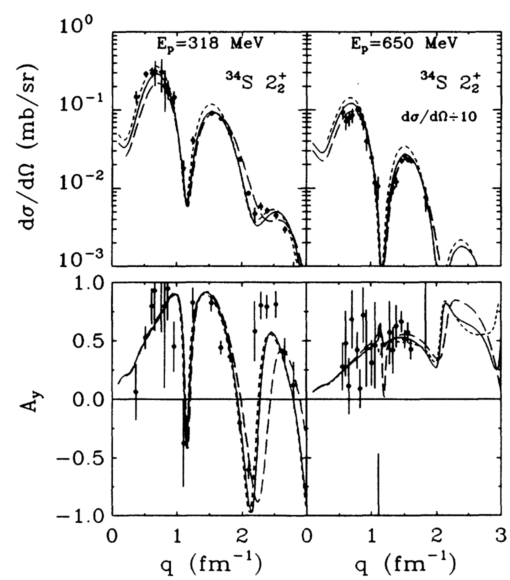

FIG. 14. Combined analysis of the 2_2^+ data: the solid lines show fits made to the two data sets simultaneously, long dashes show calculations based upon the fit to the 650 MeV data alone, and short dashes show calculations based upon the 318 MeV fit.

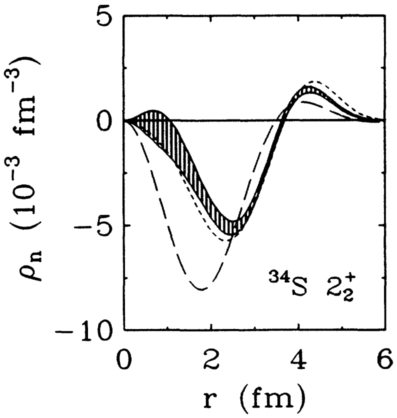

FIG. 15. The band shows ρ_n fitted to the 2_2^+ data for both 318 and 650 MeV simultaneously. The short dashes show the 318 MeV result and the long dashes the 650 MeV result. Note that the independent fits, especially at 650 MeV, should carry wider error bands but those bands are omitted for the sake of clarity.

650 MeV cross section suppresses the surface lobe and reduces M_n/M_p from 0.27(6) to 0.13(3). The density fitted to the 650 MeV data alone exhibits a larger change that results in $M_n/M_p=-0.05(7)$ consistent with zero due to the almost complete cancellation between the two lobes of the density. However, because the density itself carries quite a wide error envelope, such delicate cancellations need to be evaluated with due caution. The integral moment for such a density is obviously quite sensitive to its detailed shape and to the quality of the data. Despite the small value obtained for M_n, the neutron density still makes a large contribution to the cross section. These experiments depend most directly upon form factors for moderate momentum transfer and only indirectly upon integral quantities such as M_n.

We have previously shown that good agreement is obtained between densities fitted to ^{48}Ca(p,p') data for 200, 318, and 500 MeV [30] and for ^{88}Sr(p,p') at 200 and 500 MeV [40]. Although the consistency between ^{34}S(p,p') at 318 and 650 MeV appears to be less quantitative, renormalization of the 650 MeV data provides good qualitative consistency between the fitted densities even for the 2_2^+ state, which represents a particularly difficult case. Most of the remaining difference can be attributed to limitation of the range of momentum transfer spanned by the 650 MeV data and suspect data at the first peak of the angular distribution. Although Miskimen *et al.* [32] argue that channel coupling becomes more important as the proton energy increases, there is little apparent need to invoke large multistep contributions as suggested by Bernstein *et al.* [12]. Rather, the bimodal shape of the transition density is sufficient to explain the unusual angular distribution observed for the 2_2^+ state at both energies. Sensitivity of such weak transitions to current densities and to multistep contributions may affect the quantitative accuracy with which neutron transition densities can be extracted, but more precise and more complete data at both energies would be required to substantiate a possible spurious energy dependence of the fitted transition density. Although the moments of a bimodal density can be quite sensitive to defects of either the model or the data, the basic shape of the density and the form factor within the measured range of momentum transfer are determined more accurately and are less sensitive to such problems.

V. COMPARISON WITH PREVIOUS MOMENT DATA

The matrix elements we deduced from ^{34}S(p,p') are compared with the results of other experiments in Table IV. The M_n/M_p ratio for the lowest 2^+ state is consistent with the charge dependence of pion scattering at 50 MeV [41]. Similarly, the M_n/M_p ratios we deduced for both 2^+ states are consistent with the scattering of low-energy nucleons [15]. As discussed in Ref. [7], both of these probes enjoy excellent penetrability and are good probes of integral quantities because the long wavelengths reduce sensitivity to ambiguities in the shape of the density. On the other hand, the neutron matrix elements deduced from lifetime measurements [17] for mirror nuclei are substantially larger for both 2^+ states than the present results, although the 20–30% uncertainties are also substantial. However, Coulombic corrections to mirror matrix elements are known to reduce these ratios [42]. Recognizing that the mirror method overestimates M_n for the first 2^+ state, it is not surprising that its estimate of M_n/M_p for the second 2^+ state, which is more sensitive to Coulombic corrections by virtue of its more complicated radial shape, is also too large.

The original analysis of Bernstein *et al.* [12] assumed that the ratio R between the peak cross sections for the lowest two 2^+ states is related to their neutron and proton matrix elements according to the simple formula

$$R_{\pm}=\left[\frac{M_p(2_2^+)\pm\lambda M_n(2_2^+)}{M_p(2_1^+)+\lambda M_n(2_1^+)}\right]^2, \tag{10}$$

where λ is a measure of the ratio between the *pn* and *pp* interaction strengths and is approximately 0.81 at 650 MeV. Bernstein *et al.* assumed that the absolute values of the matrix elements could be taken directly from lifetime data for mirror transitions and compared calculations of $R_{\pm}$ based on both choices of relative sign with their experimental ratio between cross sections, $R_{\text{exp}}=0.032(3)$. The two choices gave $R_{+}=0.052(11)$ or $R_{-}=0.007(3)$, neither of which agrees with the data. If we use the values of $M_n(2_1^+)$, $M_p(2_1^+)$, and $M_p(2_2^+)$ from our work, then solving Eq. (10) gives $M_n=-0.22(18)$ as the result entered in Table IV for 650 MeV and attributed to Ref. [12]. This result is consistent with the more sophisticated LGE analysis of the 650 MeV data, presented in the preceding section, which shows that the erroneous sign results from the simplistic assumption $\rho_n\propto\rho_p$.

The results of a new experiment on ^{32,34}S$(\pi^{\pm},\pi^{\pm})$ at $E_{\pi}=50$ MeV have recently been published by Krell *et al.* [43]. Based upon 5 data for π^+ and 3 data for π^- that

TABLE IV. Summary of M_n and M_p measurements for 2^+ states in ^{34}S. Moments are given in units of fm^2 and laboratory kinetic energies K are given in MeV, when applicable. Square brackets indicate a fixed quantity used in a particular analysis. The uncertainty in the last significant figure is given in parentheses.

		2_1^+				2_2^+			
Method	K	M_p	M_n	M_0	M_n/M_p	M_p	M_n	M_0	M_n/M_p
Shell model		5.72	6.47	12.2	1.13	2.13	−1.29	0.84	−0.61
(p,p')[a]	318	[6.21(11)]	6.65(40)	12.9(4)	1.07(7)	[2.26(13)]	0.61(14)	2.87(19)	+0.27(6)
(p,p')[b]	318				1.07(10)				+0.22(6)
Lifetime[c]		6.53(13)			1.5(3)	2.18(7)			+0.55(15)
(e,e')[d]		6.21(11)				2.26(13)			
$(\pi^{\pm},\pi^{\pm})$[e]	50				1.14(8)				
$(\pi^{\pm},\pi^{\pm})$[f]	50				1.17(9)				−0.4(2)
(n,n')	21.7				1.25(35)				+0.30(18)[g]
(p,p')	29.8								+0.46(16)[h]
(p,p')[i]	650								−0.22(18)
(α,α')[j]	120	[6.25(13)]	8.55(52)	14.8(5)	1.37(9)	[2.18(7)]	0.92(41)	3.1(4)	+0.42(19)

[a]Present result based upon LGE fits to $\rho_n(r)$ combined with ρ_p from Ref. [20].
[b]Based upon scale factor fits to data for $q \le 1.0$ fm^{-1} assuming $\rho_n \propto \rho_p$.
[c]Reference [17].
[d]Reference [20].
[e]Reference [41].
[f]Reference [43].
[g]Coupled channels result from Ref. [15].
[h]Optical model result from Ref. [15].
[i]Deduced from ratio between 2_1^+ and 2_2^+ peak cross sections and Eq. (1) from Ref. [12] using present values of $M_n(2_1^+)$, $M_p(2_1^+)$, and $M_p(2_2^+)$.
[j]Based upon β_l values from Ref. [13] and lifetime results for M_p.

cover a very limited range of momentum transfer, they claim that low-energy pion scattering is consistent with $M_n/M_p = -0.4(2)$. However, they assumed $\rho_n \propto \rho_p$ and did not investigate the sensitivity of their results to shape differences. It is clear from the present results, and from exploratory calculations we have made for (π,π') at 50 MeV, that unambiguous matrix elements cannot be deduced from such limited data without knowledge of the radial densities. The assumption of proportionality between ρ_n and ρ_p cannot be justified for noncollective excitations and is often wrong. That assumption is certainly wrong for the 2_2^+ state of ^{34}S.

Finally, we consider alpha scattering at 120 MeV. Saha *et al.* [13] fitted $\beta^2 = \sigma/\sigma_{DW}$ to the data using standard Woods-Saxon optical potentials and the collective model. The isoscalar matrix element $M_0 = M_n + M_p$ can then be obtained using the Bernstein prescription [44]

$$M_0 = \frac{3A}{4\pi\hat{J}}\beta_J R^J , \tag{11}$$

where $\hat{J} = \sqrt{2J+1}$. Then, using the values of M_p determined from lifetime data, we deduce the neutron matrix elements listed in Table IV. These values differ from those originally given by Saha *et al.* for two reasons. First, the formula used in both Refs. [13] and [14] incorrectly replaces the factor of $A/\hat{J}$ in Eq. (11) by Z. Second, we followed the customary procedure of assigning R the radius of the real potential, which dominates alpha scattering at this energy, whereas Saha *et al.* used the radius of the imaginary potential. With these corrections, we obtain values of $M_0 = 14.8(5)$ and $3.1(4)$ instead of the values 16.6(6) and 3.4(4) reported by Saha *et al.* for the lowest 2^+ states seen in ^{34}S(α,α'). The new values are closer to the values 12.9(4) and 2.8(2) obtained by combining the present (p,p') results for M_n with the (e,e') results for M_p. Although the effect of these changes upon M_0 is relatively small, approximately 10% for ^{34}S, the effect upon M_n can be important because subtractions are required. Subtracting the lifetime measurements for M_p from the new M_0 values, we deduce $M_n/M_p = 1.37(9)$ and 0.41(19) from (α,α'), in good agreement with (p,p'). Note that the relatively large error bars result from subtraction of M_p from M_0 for (α,α'), whereas the (p,p') analyses fitted ρ_n directly.

However, it is well known that the Bernstein prescription suffers from ambiguities in the choice of radius and must be calibrated for each multipolarity using known transitions in nearby nuclei [45,46]. The ratio between M_0 values for two transitions in the same nucleus is independent of R and hence should be less model dependent. For 120 MeV (α,α'), we deduce $M_0(2_2^+)/M_0(2_1^+) = 0.21(3)$, which agrees very well with the present (p,p') result 0.22(2).

Therefore, when reasonable allowances are made for model dependences and differing radial sensitivities, we find no serious discrepancies between the present results and those listed in Table IV. The two analyses, which obtain a relative negative sign between the neutron and proton matrix elements for the 2_2^+ state of ^{34}S, were both based upon the misleading assumption of proportionality between corresponding densities. That assumption is not justified for noncollective transitions. We consider the present analysis to be definitive because it eliminates arbitrary assumptions concerning radial densities, minimizes model dependence, and utilizes a relatively penetrating probe.

VI. RESULTS FOR NEGATIVE-PARITY STATES

Neither electron scattering data nor shell-model calculations are available for the negative-parity states of ^{34}S, but the data for these states appear quite similar to the data for corresponding states in ^{32}S. Therefore, in Fig. 16 we compare the data for 1_1^-, 3_1^-, and 5_1^- states of ^{34}S with the fits made for ^{32}S and deduce scale factors between the cross sections for corresponding states of these isotopes. For all three states, we find that the analyzing power angular distributions are essentially independent of isotope and that cross sections for ^{34}S, relative to those for ^{32}S, differ only by scale factors of about 0.80, 1.15, and 0.95 for the 1_1^-, 3_1^-, and 5_1^- states, respectively. The most significant deviations occur for the 5^- analyzing power, but we note that very similar deviations between this fit and the data for ^{32}S are also seen in Ref. [10]. Therefore, the structures of low-lying negative-parity transitions appear little changed by the addition of two $d_{3/2}$ neutrons. Although the data obtained for second 1^-, 3^-, and 5^- states are sparse, there are indications of significant form factor differences between the lowest and higher negative-parity states.

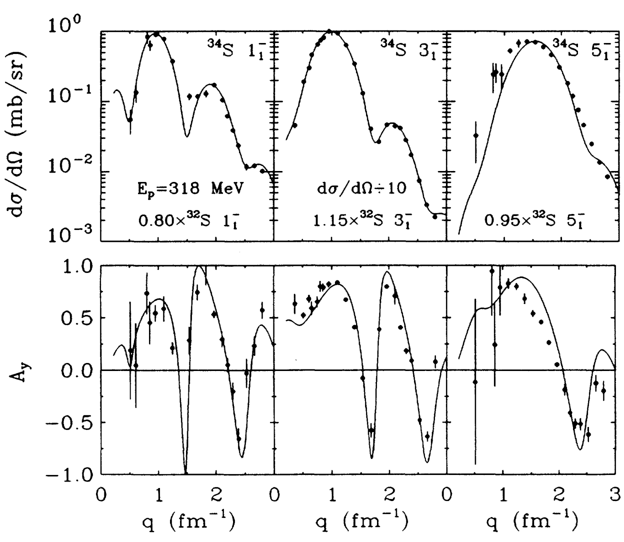

FIG. 16. Data for negative-parity states of ^{34}S are compared with fits made to the corresponding data for ^{32}S. Cross sections for the lowest 1^-, 3^-, and 5^- states of ^{34}S are related by factors of 0.80, 1.15, and 0.95 to corresponding ^{32}S cross sections, but the angular distributions are very similar.

VII. SUMMARY AND CONCLUSIONS

We have obtained cross section and analyzing power data for ^{34}S(p,p') at 318 MeV and compared the data for positive-parity states with shell-model calculations based upon the USD interaction. We find that the shell model provides good agreement with the data for the 2_1^+ state but predicts much smaller cross sections and a very different angular distribution than observed for the 2_2^+ state. Similarly, the strengths predicted for the 2_3^+, 2_4^+, and 4_1^+ states need considerable enhancement to reproduce the data and the 2_3^+ angular distribution indicates a substantial discrepancy in the shape of the shell-model density. We also find that angular distributions for excitation of corresponding negative-parity states of ^{34}S and ^{32}S are quite similar, differing only by scale factors near unity.

Neutron transition densities were fitted to the data for the 2_1^+ and 2_2^+ states using an empirical effective interaction previously calibrated upon ^{16}O and ^{40}Ca data and procedures demonstrated to produce accurate results for densities fitted to ^{32}S(p,p') data. We find that the shell model describes both proton and neutron densities for the lowest 2^+ state quite well, but is lacking an important surface feature for the 2_2^+ neutron density revealed by the unusual ^{34}S$(p,p')2_2^+$ angular distribution. The fitted density gives $M_n/M_p=+0.27(6)$, which should be compared with -0.61 for the shell model and $+0.55(15)$ from electromagnetic lifetime measurements in the $A=34$ triplet. The positive sign agrees with (α,α') and (n,n') results, but disagrees with the original interpretation of data for 650 MeV protons. However, the present densities give a much better description of the $E_p=650$ MeV data than either the shell model or the original analysis.

The relatively small neutron matrix element for the 2_2^+ state is due to the delicate cancellation between the two lobes of the transition density and does not indicate an intrinsically small neutron contribution. On the contrary, the neutron density is similar in size to the proton density, but different in shape, and makes a comparable contribution to the differential cross section for excitation by proton scattering. Simplistic assumptions concerning transition densities often fail for noncollective excitations and in this case account for the considerable spread among previous determinations of M_n for this transition. By eliminating arbitrary assumptions concerning the radial density and minimizing model dependence, we have measured the shape of $\rho_n(r)$ for the 2_2^+ state and have obtained a more reliable value of M_n.

The measured shape of ρ_n for the 2_2^+ state of ^{34}S is difficult to reproduce within the confines of the *sd* shell and suggests participation of $(f_{7/2})^2$ configurations. In particular, the bimodal shape of ρ_n cannot be reproduced with the *sd* shell without an unreasonably large change in the oscillator parameter but can be reproduced by inclusion of an $(f_{7/2})^2$ contribution. We also find that shell-model calculations for 4^+ states give cross sections in qualitative agreement with the (p,p') data for ^{32}S but much smaller than the data for ^{34}S. Similar results are also obtained for the silicon isotopes. These results suggest that either the shell-model isovector interaction or the assumption of charge-independent core polarization is incorrect, especially for $C4$ excitations.

Using complementary (e,e') and (p,p') experiments it is now possible to measure both proton and neutron transition densities for normal-parity excitations with good accuracy and to critically evaluate the isospin structure of shell-model calculations. Radial neutron densities often provide much more insight into the structure of a transition than can be obtained from the less discriminating information provided by scaling or collective model analyses of data for strongly absorbed probes. To understand these radial densities it will be necessary to examine the scope of the model space and to improve the model for core polarization.

ACKNOWLEDGMENTS

We thank W. Lozowski of the Indiana University Cyclotron Facility for fabrication of the sulfur targets. We also thank Dr. J. Carr for valuable criticism of the manuscript. One of the authors (H.S.) was supported in part by the National Research Council–NASA. This work was supported in part by grants from the National Science Foundation and the U.S. Department of Energy.

---

*Present address: Department of Physics, American University, Washington, D.C. 20016.

†Present address: NIH, Bethesda, MD 20892.

‡Present address: NASA–Goddard Space Flight Center, Greenbelt, MD 20771.

[1] B. A. Brown, R. Radhi, and B. H. Wildenthal, Phys. Rep. **101**, 313 (1983).

[2] B. A. Brown and B. H. Wildenthal, Annu. Rev. Nucl. Part. Sci. **38**, 29 (1988).

[3] T. T. S. Kuo, Nucl. Phys. **A103**, 71 (1967); T. T. S. Kuo and G. E. Brown, Nucl. Phys. **85**, 40 (1966).

[4] A. M. Bernstein, V. R. Brown, and V. A. Madsen, Phys. Rev. Lett. **42**, 425 (1979).

[5] A. M. Bernstein, V. R. Brown, and V. A. Madsen, Phys. Lett. **103B**, 255 (1981).

[6] J. J. Kelly, Phys. Rev. C **37**, 520 (1988).

[7] J. A. Carr, F. Petrovich, and J. Kelly, in *Neutron-Nucleus Collisions—A Probe of Nuclear Structure,* edited by J. Rapaport, R. W. Finlay, S. M. Grimes, and F. Dietrich, AIP Conf. Proc. No. 124 (AIP, New York, 1985), p. 230.

[8] J. J. Kelly, W. Bertozzi, T. N. Buti, J. M. Finn, F. W. Hersman, M. V. Hynes, C. Hyde-Wright, B. E. Norum, A. D. Bacher, G. T. Emery, C. C. Foster, W. P. Jones, D. W. Miller, B. L. Berman, J. A. Carr, and F. Petrovich, Phys. Lett. **169B**, 157 (1986).

[9] J. J. Kelly, Q. Chen, P. P. Singh, M. C. Radhakrishna, and W. P. Jones, Phys. Rev. C **41**, 2525 (1990).

[10] J. J. Kelly, M. A. Khandaker, P. Boberg, A. E. Feldman, B. S. Flanders, S. Hyman, H. Seifert, P. Karen, B. E. Norum, P. Welch, S. Nanda, and A. Saha, preceding paper, Phys. Rev. C **44**, 1693 (1991).

[11] B. A. Brown, B. H. Wildenthal, W. Chung, S. E. Massen, M. Bernas, A. M. Bernstein, R. Miskimen, V. R. Brown, and V. A. Madsen, Phys. Rev. C **26**, 2247 (1982).

[12] A. M. Bernstein, R. A. Miskimen, B. Quinn, S. A. Wood, M. V. Hynes, G. S. Blanpied, B. G. Ritchie, and V. R. Brown, Phys. Rev. Lett. **49**, 451 (1982).

[13] A. Saha, K. K. Seth, M. Artuso, B. Harris, R. Seth, H. Nann, and W. W. Jacobs, Phys. Rev. Lett. **52**, 1876 (1984).

[14] A. Saha, K. K. Seth, D. Barlow, H. Nann, and W. W. Jacobs, Phys. Lett. **114B**, 419 (1982).

[15] R. Alarcon, J. Rapaport, R. T. Kouzes, W. H. Moore, and B. A. Brown, Phys. Rev. C **31**, 697 (1985); R. Alarcon and J. Rapaport, Nucl. Phys. **A458**, 502 (1986).

[16] P. M. Endt, At. Data Nucl. Data Tables **23**, 3 (1979).

[17] J. Keinonen, A. Luukkainen, and M. Bister, Nucl. Phys. **A412**, 101 (1984).

[18] J. J. Kelly, A. E. Feldman, B. S. Flanders, H. Seifert, D. Lopiano, B. Aas, A. Azizi, G. Igo, G. Weston, C. Whitten, A. Wong, M. V. Hynes, J. McClelland, W. Bertozzi, J. M. Finn, C. E. Hyde-Wright, R. W. Lourie, P. E. Ulmer, B. E. Norum, and B. L. Berman, Phys. Rev. C **43**, 1272 (1991).

[19] J. J. Kelly, P. Boberg, A. E. Feldman, B. S. Flanders, M. A. Khandaker, S. D. Hyman, H. Seifert, P. Karen, B. E. Norum, P. Welch, S. Nanda, and A. Saha, Phys. Rev. C (to be published).

[20] U. Wörsdörfer, H. J. Emrich, H. Miska, D. Rychel, R. Gyufko, and C. A. Wiedner, Nucl. Phys. **A438**, 711 (1985).

[21] W. D. M. Rae, A. Etchegoyen, and B. A. Brown, computer program OXBASH (unpublished).

[22] G. E. Brown, *Unified Theory of Nuclear Models and Nucleon-Nucleon Forces* (North-Holland, Amsterdam, 1967).

[23] F. Petrovich, H. McManus, J. Borysowicz, and G. R. Hammerstein, Phys. Rev. C **16**, 839 (1977).

[24] L. J. Tassie, Austr. J. Phys. **9**, 407 (1956); **26**, 433 (1973).

[25] F. Petrovich, R. J. Philpott, A. W. Carpenter, and J. A. Carr, Nucl. Phys. **A425**, 609 (1984).

[26] D. Rychel, Ph.D. thesis, University of Mainz, 1983; H. deVries, C. W. deJager, and C. deVries, At. Data Nucl. Data Tables **36**, 495 (1987).

[27] M. A. Franey and W. G. Love, Phys. Rev. C **31**, 488 (1985).

[28] L. Ray, Phys. Rev. C **41**, 2816 (1990).

[29] H. V. von Geramb, in *The Interaction Between Medium Energy Nucleons in Nuclei–1982,* edited by H. O. Meyer, AIP Conf. Proc. No. 97 (AIP, New York, 1983), p. 44; L. Rikus, K. Nakano, and H. V. von Geramb, Nucl. Phys. **A414**, 413 (1984).

[30] A. E. Feldman, P. Boberg, B. S. Flanders, S. D. Hyman, J. J. Kelly, M. A. Khandaker, H. Seifert, P. Karen, B. E. Norum, P. Welch, A. Saha, S. Nanda, Q. Chen, and A. Scott, Bull. Am. Phys. Soc. **35**, 1038 (1990); A. E. Feldman, Ph.D. thesis, University of Maryland, 1991.

[31] J. Heisenberg, computer program FOUBES (unpublished); J. Heisenberg, Adv. Nucl. Phys. **12**, 61 (1981).

[32] R. A. Miskimen, A. M. Bernstein, G. Bernhardt, C. F. Williamson, B. A. Brown, and R. Alarcon, Phys. Rev. C **37**, 1600 (1988).

[33] R. A. Miskimen, A. M. Bernstein, B. Quinn, S. A. Wood, M. V. Hynes, G. S. Blanpied, B. G. Ritchie, and V. R. Brown, Phys. Lett. **131B**, 26 (1983).

[34] R. A. Miskimen, Ph.D. thesis, MIT, 1983.

[35] L. G. Arnold, B. C. Clark, R. L. Mercer, and P. Schwandt, Phys. Rev. C **23**, 1949 (1981).

[36] B. S. Flanders, J. J. Kelly, H. Seifert, D. Lopiano, B. Aas, A. Azizi, G. Igo, G. Weston, C. Whitten, A. Wong, M. V. Hynes, J. McClelland, W. Bertozzi, J. M. Finn, C. E. Hyde-Wright, R. W. Lourie, B. E. Norum, P. Ulmer, and B. L. Berman, Phys. Rev. C **43**, 2103 (1991).

[37] S. Hama, B. C. Clark, E. D. Cooper, H. S. Sherif, and R. L. Mercer, Phys. Rev. C **41**, 2737 (1990).

[38] N. Ottenstein, S. J. Wallace, and J. A. Tjon, Phys. Rev. C **38**, 2272, 2289 (1988).

[39] E. Bleszynski, B. Aas, D. Adams, M. Bleszynski, G. J. Igo, T. Jaroszewicz, A. Ling, D. Lopiano, F. Sperisen, M. G. Moshi, C. A. Whitten, K. Jones, and J. B. McClelland, Phys. Rev. C **37**, 1527 (1988).

[40] B. S. Flanders, J. J. Kelly, K. K. Seth, B. Parker, M. Artuso, R. Soundranayagm, F. W. Hersman, and J. P. Connelly, Bull. Am. Phys. Soc. **32**, 1121 (1987); F. W. Hersman, J. R. Calarco, J. Heisenberg, T. Milliman, J. J. Kelly, A. Scott, F. T. Baker, V. Penumetcha, A. Bacher, G. T. Emery, C. Olmer, W. Jones, and M. Grimm, *ibid.* **29**, 628 (1984).

[41] R. J. Sobie, T. E. Drake, K. L. Erdman, R. R. Johnson, H. W. Roser, R. Tacik, E. W. Blackmore, D. R. Gill, S. Martin, C. A. Wiedner, and T. Masterson, Phys. Rev. C **30**, 1612 (1984).

[42] B. A. Brown, A. Arima, and J. B. McGrory, Nucl. Phys. **A277**, 77 (1977).

[43] S. Krell, B. M. Barnett, H. Clement, J. Jaki, R. R. Johnson, C. Joram, W. Kluge, H. Matthäy, M. Metzler, D. Renker, and G. J. Wagner, Europhys. Lett. **15**, 11 (1991).

[44] A. M. Bernstein, Adv. Nucl. Phys. **3**, 325 (1969).

[45] H. Rebel, Z. Phys. A **277**, 35 (1976); H. Rebel, R. Pesl, H. J. Gils, and E. Friedman, Nucl. Phys. **A368**, 61 (1981).

[46] G. J. Wagner, P. Grabmayr, and H. R. Schmidt, Phys. Lett. **113B**, 447 (1982).